Electronic Supplementary Material (ESI) for Journal of Materials Chemistry A.

Supporting Information

Polyamino acid with zincphilic chains enabling high-performance Zn anode

Jiaxing Liu,[a,b] Weihao Song,[a,b] Yili Wang,[a,b] Shuaize Wang,[a,b] Tianren Zhang,[c] Yinliang Cao,[c] Shuguo Zhang,[c] Chunchuan Xu,[c] Yongzheng Shi,[a,b] Jin Niu, [a,b,*] Feng Wang[a,b,*]

[a] State Key Laboratory of Chemical Resource Engineering, Laboratory of Electrochemical Process and Technology for materials, Beijing University of Chemical Technology, Beijing, 100029, P. R. China

[b] Beijing Advanced Innovation Center for Soft Matter Science and Engineering, Beijing University of Chemical Technology, Beijing, 100029, P. R. China

[c] Tianneng Battery Group Co.,Ltd. Zhejiang, 313100, P. R. China

Material Characterization

The morphology of materials and anodes were characterized by SEM (JEOL, JSM-6701F) and EDS were used to determine the elemental distribution of the Zn-anode surface. XRD patterns were recorded on a SHIMADZU XRD diffra-7000 X-RAY diffractometer. Raman spectra were characterized using a LabRam HR800 spectrometer. FTIR spectra were measured by a PerkinElmer Spectrum 100 spectrometer. The surface chemical compositions of the materials were analyzed by XPS (ESCALAB 250). In-situ optical microscopy analyses were carried on an optical microscope (XJ-550) with an electrolytic cell (Beijing Science Star Technology). Hydrogen evolution was quantified by in-situ electrochemical gas chromatography (SHIMADZU GC-2030). The sessile drop contact angle was measured on a contact angle measuring instrument (DataPhysics OCA20).

DFT calculations

The DFT calculation was performed by the Vienna Ab-initio Simulation Package (VAA), and the exchange-correlation energy was approximately described by the Perdew-Burke-Ernzerhof (PBE) functional based on the generalized gradient approximation (GGA) [S1]. In all calculation, a cutoff energy with the value of 400 eV was used for the plane wave basis, and the convergence criteria for the ionic relaxation and the electronic self-consistent calculation were set to 0.02 eV $Å^{-1}$ and 10^{-5} eV, respectively. The long-range dispersion correction for the van der Waals interaction was implemented through the DFT-D3 method in all calculation. It should be noted that a trimer was used to represent PAA for calculation.

Electrochemical measurements

Zn symmetric cells were assembled by sandwiching the glass fiber separator between commercial Zn plates in CR2032-type cells filled with different electrolytes. Coulombic efficiency was measured in the Zn-Cu half cells, which were assembled using Cu plate as working electrode, Zn plate as counter electrode, and glass fiber as separator, respectively. The Zn-MnO_2 full cells (including coin cell and pouch cell) were assembled using Zn anode and MnO_2 cathode. The diameter of the Zn plates is 10 mm with a thickness of 100 μm. Before use, the Zn plates were polished using

sandpapers (1000 mesh and 2000 mesh), followed by water/ethanol washing for several times. The electrolyte amount for the half cell and full cell were 100 μL and ~15 μL mg^{-1} (based on the weight of cathode materials), respectively. The cathode was prepared by mixing MnO_2 nanorods (Fig. S8, S9), acetylene black, and polyvinylidene fluoride in a weight ratio of 7: 2: 1 with N-methyl-2-pyrrolidone as a solvent. The obtained slurry was cast onto a Ti foil, followed by drying at 120 °C for 16 h under vacuum. The loading weight of the cathode is ~3 mg cm^{-2}.

Tafel plot, LSV, CA, and CV measurements were performed using Zn plates as both the working electrode and the counter electrode, and Ag/AgCl electrode as the reference electrode, respectively. The Tafel plots were measured by scanning between −0.6 V and −1.6 V at 10 mV s^{-1}. The chronoamperometry were measured at a fixed overpotential of −150 mV.

For the in-situ electrochemical gas chromatography, a two-neck bottle with two Zn electrodes was applied for measurement (Fig. S22). N_2 was passed into the two-neck bottle to take out the produced gas. The gas chromatography was used to quantitatively determine the real-time hydrogen production by controlling the same gas inlet flow and sampling time.

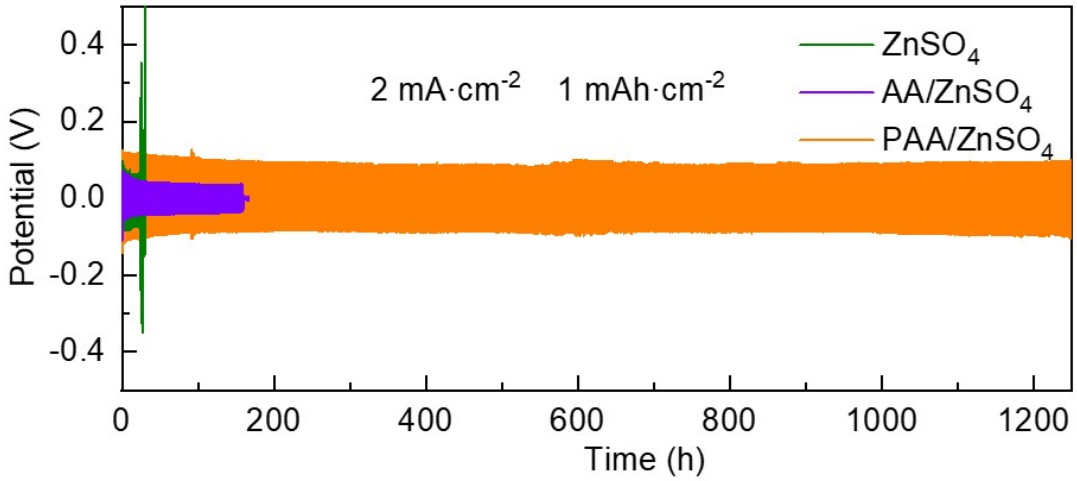

Fig. S1. The voltage profiles of the Zn|Zn cells tested in the $ZnSO_4$, $AA/ZnSO_4$, and $PAA/ZnSO_4$ electrolytes at the current density of 2 mA cm^{-2} with the capacity of 1 mAh cm^{-2}.

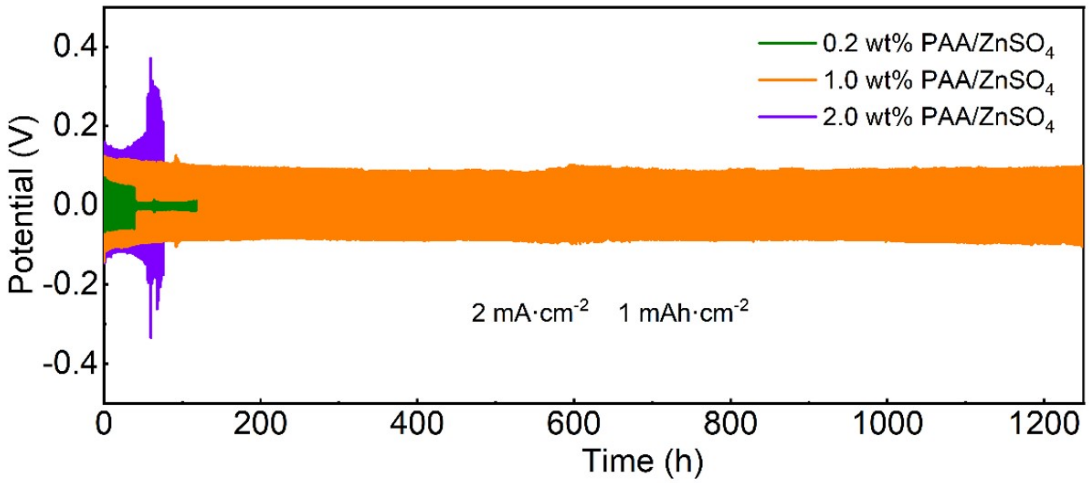

Fig. S2. The voltage profiles of the Zn|Zn cells tested in the PAA/$ZnSO_4$ electrolytes with different amount of PAA at the current density of 2 mA cm^{-2} with the capacity of 1 mAh cm^{-2}.

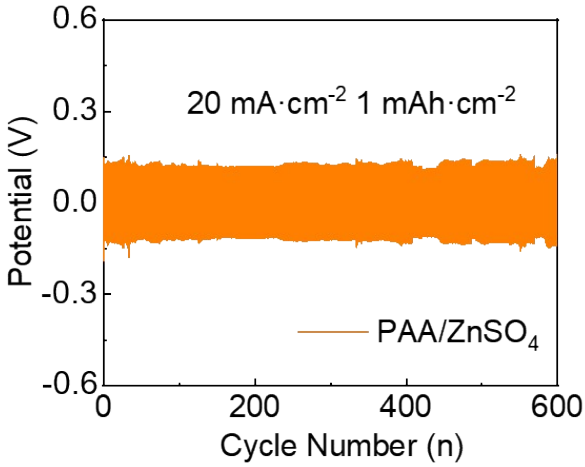

Fig. S3. The voltage profile of the Zn|Zn cell tested in the PAA/$ZnSO_4$ electrolyte at the current density of 20 mA cm^{-2} with the capacity of 1 mAh cm^{-2}.

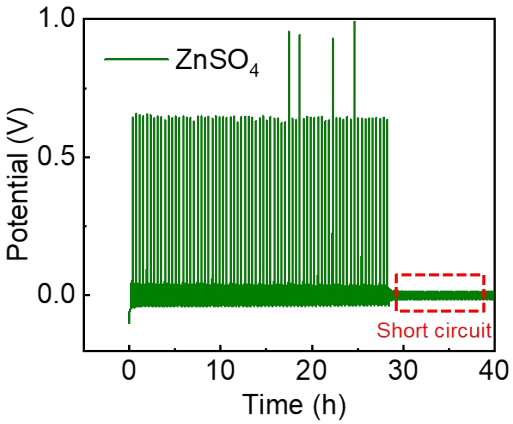

Fig. S4. The potential-time curve of Zn|Cu cell tested in $ZnSO_4$ electrolyte at the current density of 10 mA cm^{-2} with the capacity of 2 mAh cm^{-2}

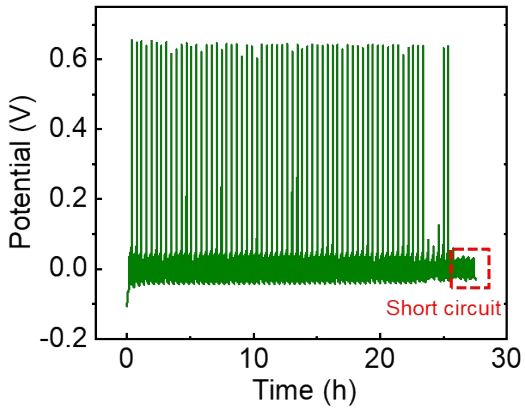

Fig. S5 The potential-time curve of Zn|Cu cell tested in AA/$ZnSO_4$ electrolyte at the current density of 10 mA cm^{-2} with the capacity of 2 mAh cm^{-2}.

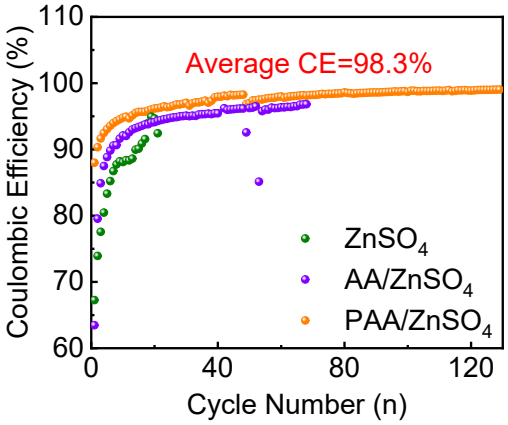

Fig. S6. The coulombic efficiency of the Zn|Cu half cells using the $ZnSO_4$, $AA/ZnSO_4$, and $PAA/ZnSO_4$ electrolytes at the current density of 2 mA cm^{-2} with the capacity of 1 mAh cm^{-2}.

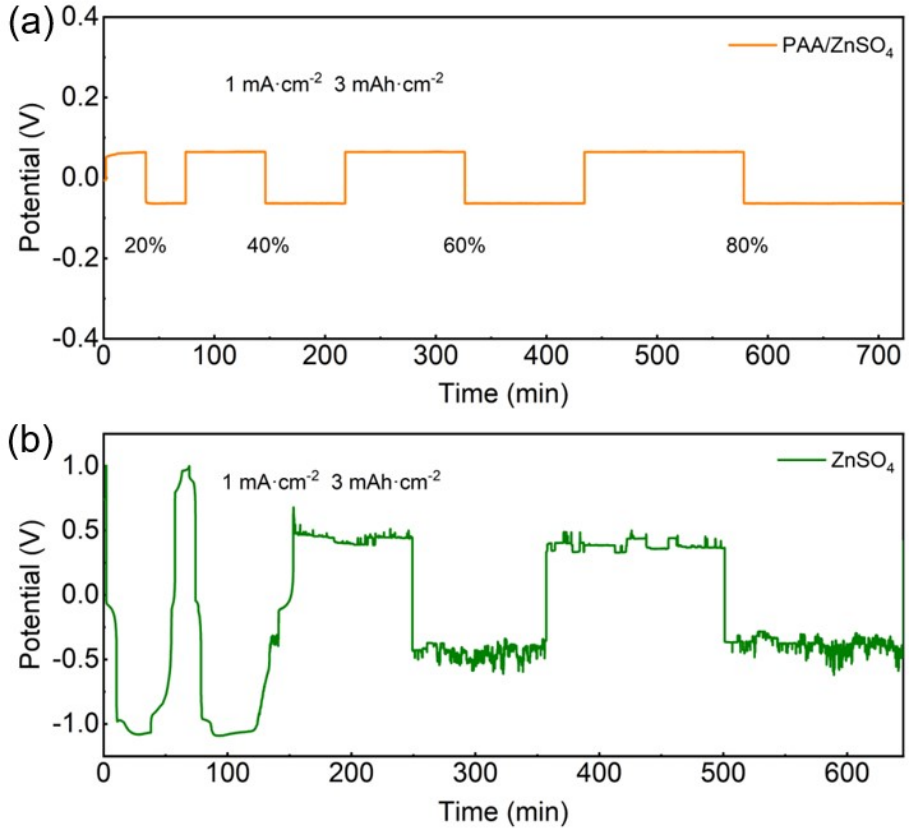

Fig. S7. The charge/discharge profiles of the Zn|Zn cells in the (a) PAA/$ZnSO_4$ and (b) $ZnSO_4$ electrolytes under different depth-of-discharge.

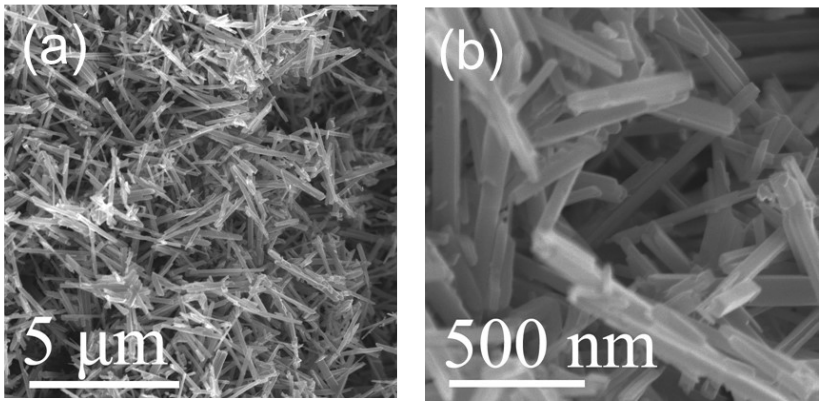

Fig. S8. The SEM images of MnO_2 nanorods.

For the preparation of MnO_2 nanorods, 6 mmol $KMnO_4$ was dissolved in 60 mL deionized water and then 20 mmol concentrated HCl was slowly added into the solution under vigorous stirring. The resultant transparent purple solution was transferred into a 100 mL Teflon-lined stainless-steel autoclave. The sealed autoclave was heated to 140 °C and maintained for 12 h.

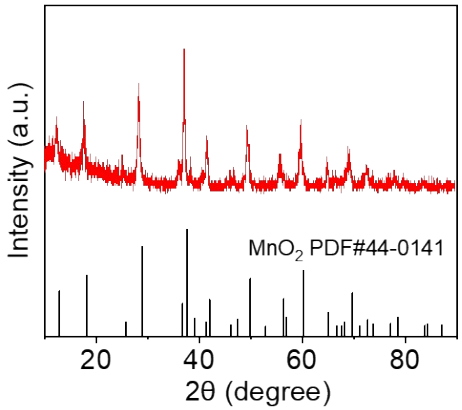

Fig. S9. The XRD pattern of MnO_2 nanorods.

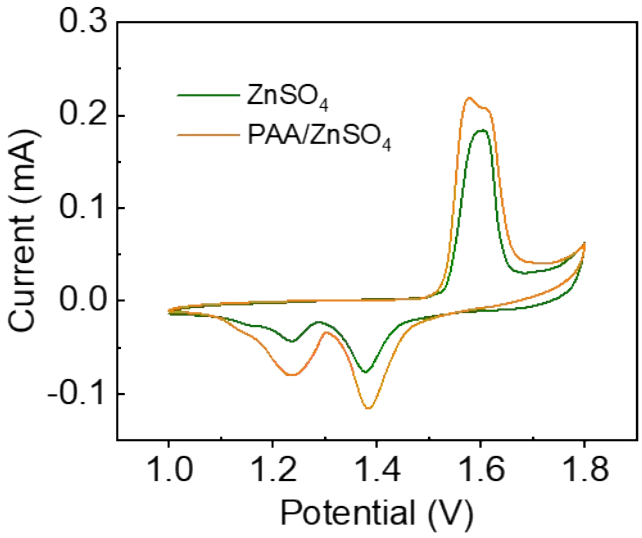

Fig. S10. The CV curves of the Zn-MnO_2 full cells using the PAA/$ZnSO_4$ electrolyte and $ZnSO_4$ electrolyte.

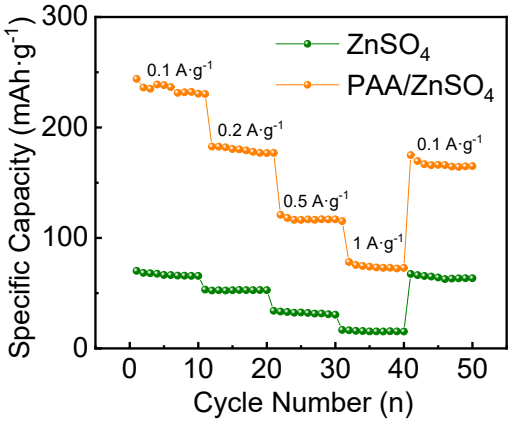

Fig. S11. Rate performance of the Zn-MnO_2 full cells after 100 cycles at 0.2 A g^{-1} using the PAA/$ZnSO_4$ electrolyte and $ZnSO_4$ electrolyte.

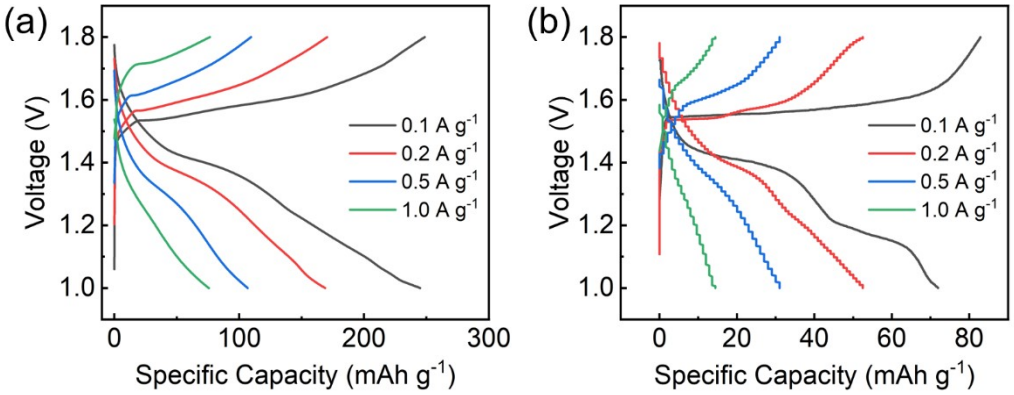

Fig. S12. The charge/discharge profiles of the Zn/MnO_2 cells in the (a) PAA/$ZnSO_4$ and (b) $ZnSO_4$ electrolytes.

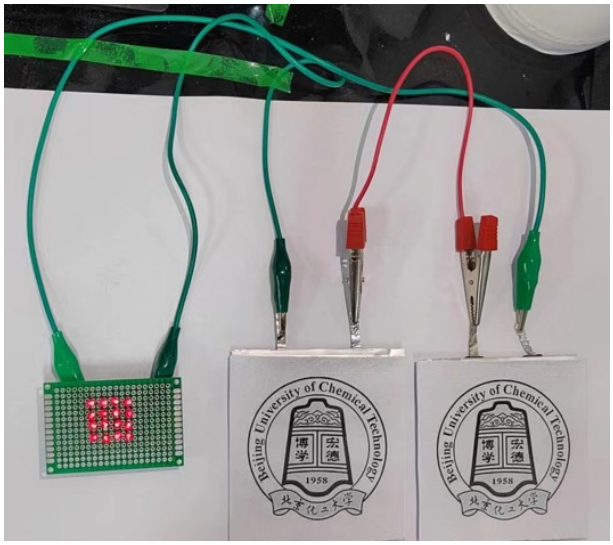

Fig. S13. The connection between the pouch cells and the LEDs.

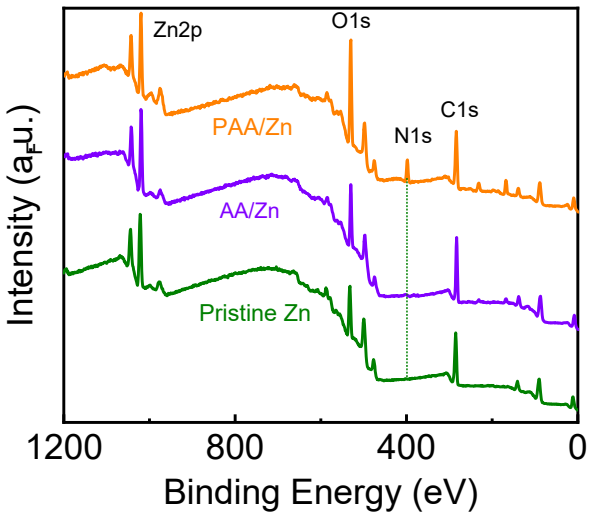

Fig. S14. The XPS spectra of pristine Zn anode and Zn anodes after 10 cycles in the PAA and AA additives.

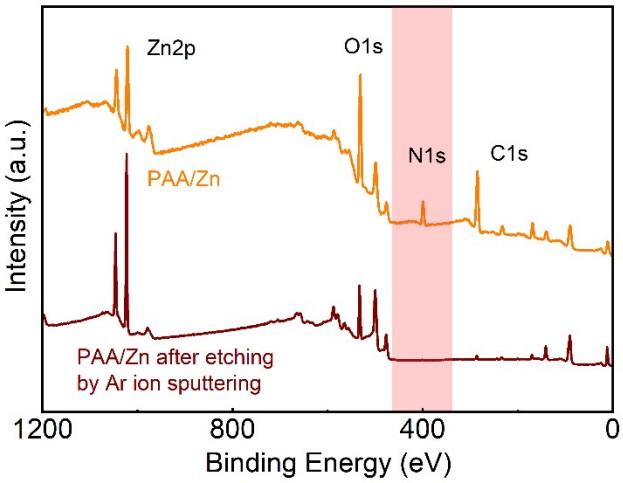

Fig. S15. XPS spectra of the cycled Zn anode (with a plating capacity of 1 mAh cm^{-2}) in the PAA/$ZnSO_4$ electrolyte before and after etching by Ar ion sputtering.

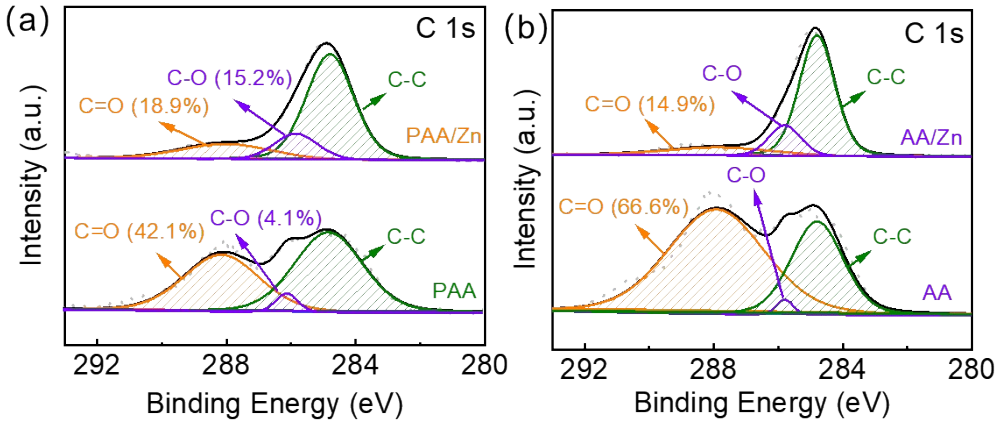

Fig. S16. The high-resolution C1s XPS spectra for (a) PAA and PAA/Zn, (b) AA and AA/Zn.

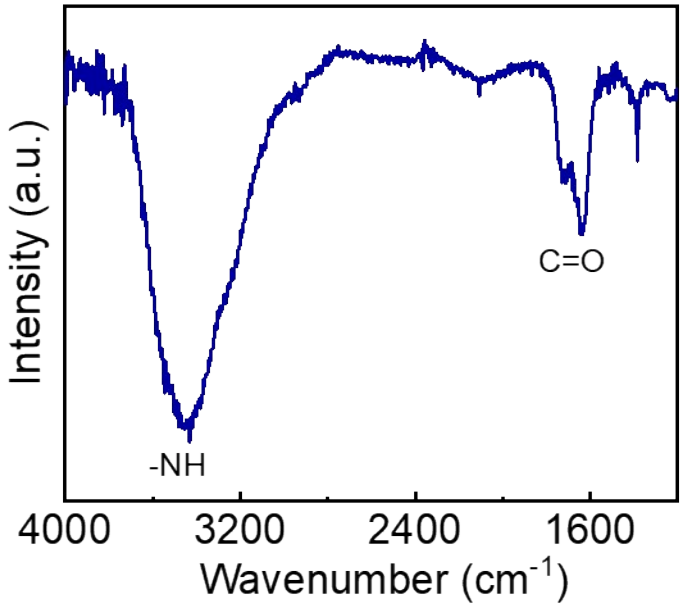

Fig. S17. The FTIR spectrum of PAA.

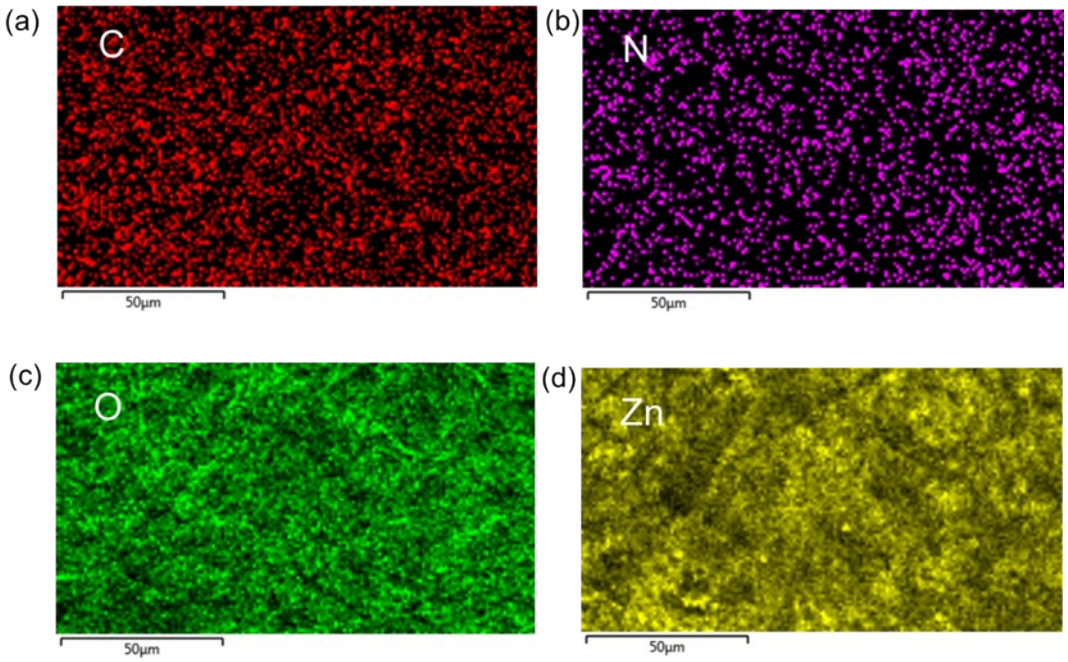

Fig. S18. The mapping images using the X-ray energy dispersive spectroscopy of PAA/Zn.

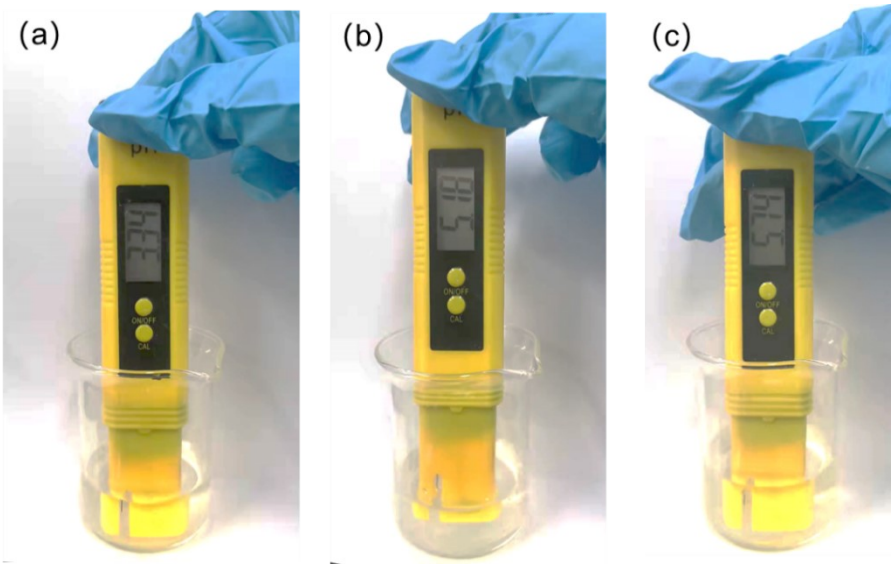

Fig. S19. The pH of the (a) AA/$ZnSO_4$, (b) PAA/$ZnSO_4$, and (c) 2 M $ZnSO_4$ electrolytes.

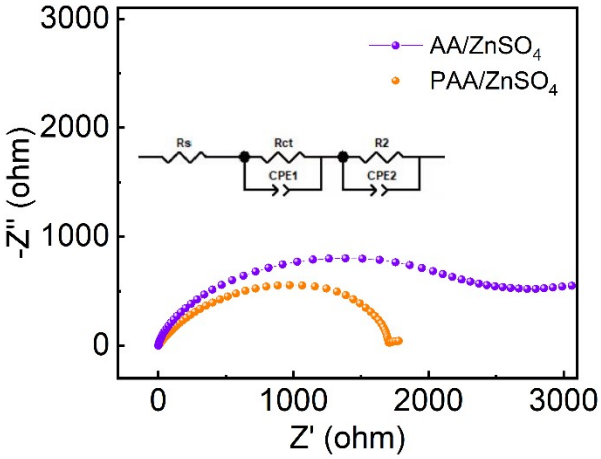

Fig. S20. The electrochemical impedance spectroscopy results of the Zn|Zn cells tested in the PAA/$ZnSO_4$ and AA/$ZnSO_4$ electrolytes (inset: equivalent circuit for fitting).

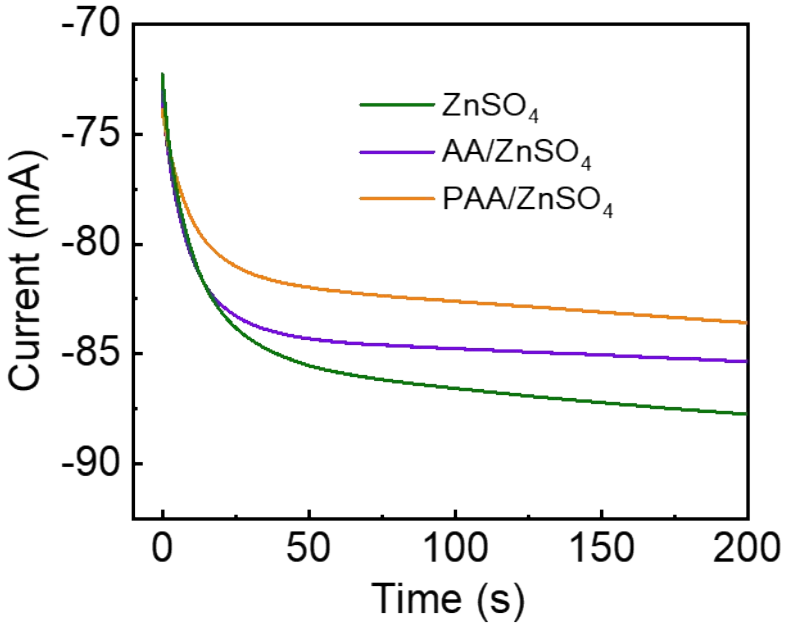

Fig. S21. The potentiostatic current-time transient curve of Zn plate tested in the $ZnSO_4$, $AA/ZnSO_4$, and $PAA/ZnSO_4$ electrolytes at a fixed overpotential of −150 mV.

Fig. S22. Photo of in-situ electrochemical gas chromatography device.

Table S1. Comparison of the electrochemical performance of Zn anode in aqueous electrolytes with previous works.

Main materials	Current density and areal capacity	Cycle Time	Reference[a]
PAA	**1 mA·cm^{-2}, 1 mAh·cm^{-2}**	**2200 h**	**This work**
	2 mA·cm^{-2}, 1 mAh·cm^{-2}	**1200 h**	
	10 mA·cm^{-2}, 1 mAh·cm^{-2}	**360 h**	
	5 mA·cm^{-2}, 3 mAh·cm^{-2}	**300 h**	
$Zn_{88}Al_{12}$ alloy	0.5 mA·cm^{-2}, 0.5 mAh·cm^{-2}	2000 h	[9]
Zn@ZnO	0.2 mA·cm^{-2}, 0.2 mAh·cm^{-2}	1000 h	[12]
	5 mA·cm^{-2}, 2.5 mAh·cm^{-2}	100 h	
TiO_2	1 mA·cm^{-2}, 1 mAh·cm^{-2}	460 h	[32]
TiO_2/PVDF	0.885 mA·cm^{-2}, 0.885 mAh·cm^{-2}	2000 h	[33]
Acetonitrile	2 mA·cm^{-2}, 1 mAh·cm^{-2}	580 h	[34]
MXene/ZnS	1 mA·cm^{-2}, 1 mAh·cm^{-2}	1100 h	[35]
	10 mA·cm^{-2}, 1 mAh·cm^{-2}	180 h	
Functional supramolecules	1 mA·cm^{-2}, 1 mAh·cm^{-2}	2000 h	[36]
	5 mA·cm^{-2}, 3 mAh·cm^{-2}	250 h	
Cyanoacrylate	0.5 mA·cm^{-2}, 0.5 mAh·cm^{-2}	800 h	[37]
$NaTi_2(PO_4)_3$	1 mA·cm^{-2}, 1 mAh·cm^{-2}	260 h	[38]
Zn/CNT	2 mA·cm^{-2}, 2 mAh·cm^{-2}	200 h	[39]
	5 mA·cm^{-2}, 2.5 mAh·cm^{-2}	110 h	
Zinc alginate gel	1.7 mA·cm^{-2}, 0.885 mAh·cm^{-2}	270 h	[40]
	8.8 mA·cm^{-2}, 2.2 mAh·cm^{-2}	200 h	
Collagen hydrolysate	1 mA·cm^{-2}, 1 mAh·cm^{-2}	60 h	[41]
Electrodeposition Zn	10 mA·cm^{-2}, 1.8 mAh·cm^{-2}	200 h	[42]
MXene	0.2 mA·cm^{-2}, 0.2 mAh·cm^{-2}	800 h	[43]

[a]The reference numbers are same to those in the manuscript.

Table S2. Element content and percentage of total N1s, C1s, Zn2p analyzed by XPS.

	Element content %				% of total C1s			% of total N1s		% of total Zn2p	
	C	N	O	Zn	C=O	C-O	C-C	-NH-CO-	N-Zn	Zn-O	Zn
PAA	33.4	3.2	63.4	-	42.1	4.1	53.8	100	-	-	-
PAA/Zn	54.1	2.4	35.6	7.8	18.9	15.2	65.9	12.8	87.2	89.1	10.9
AA/Zn	62.7	2.0	24.9	10.4	14.9	16.6	68.5	-	-	82.0	18.0

References

[S1] C. Huang; X. Zhao; S. Liu; Y. Hao; Q. Tang; A. Hu; Z. Liu; X. Chen, *Adv Mater* **2021,** *33*, e2100445.